Chapter 4

Performance of the LHCf detectors

4.1 Expected performance of the LHCf detectors

Here we present the results of Monte Carlo studies for evaluating the performance of the LHCf detectors described in section 2. Detector performance was also checked by beam tests described later in section 4.2 In these studies, EPICS [20], which is widely used in air shower experiments, was used for detector simulation. EPICS simulates all electromagnetic and hadronic processes which have been well benchmarked by results from EGS4 or CERN test beam experiments. The primary hadronic interaction model used in this section is DPMJET3 [21] which is also commonly used in air shower simulations.

Energy resolution

The LHCf detectors consist of tungsten sampling shower calorimeters ($44\,X_0$ and $1.7\,\lambda$) with compact apertures which results in shower particle leakage from the edges of the calorimeters.

The number of shower particles contained in calorimeter is plotted in figure 4.1 as a function of the distance between the shower center and the nearest edge. Though the leakage fraction is not negligible, we have found that it does not depend on the energy of the incident primary particle. Using the shower position measured by the position sensitive layers together with the leakage function in figure 4.1, the measured shower energy can be corrected for shower leakage.

The expected energy resolution of the $20\,\mathrm{mm}\times20\,\mathrm{mm}$ calorimeter after shower leakage correction is plotted in figure 4.2 as a function of incident γ-ray energy. Here the γ-ray energy is reconstructed from the energy deposited by shower particles after the 3rd tungsten layer (at $6\,X_0$) in order to prevent contamination due to background of low energy γ-rays. Selecting events with shower axis 2 mm or more from the nearest edge of the calorimeter and applying the leakage correction, the expected energy resolution is 6.3% for 100 GeV and 2.8% for 1 TeV γ-rays.

While the total length of the calorimeters expressed in nuclear interaction lengths is small ($1.7\,\lambda$), the detector still can be used as a hadron shower calorimeter. To minimize longitudinal shower leakage, events are selected which start their shower development near the front of the detector. Selecting events for which the shower axis is 2 mm or more from the closest edge, and requiring that the energy deposited in the first radiation length exceeds that deposited by 20 MIPs,

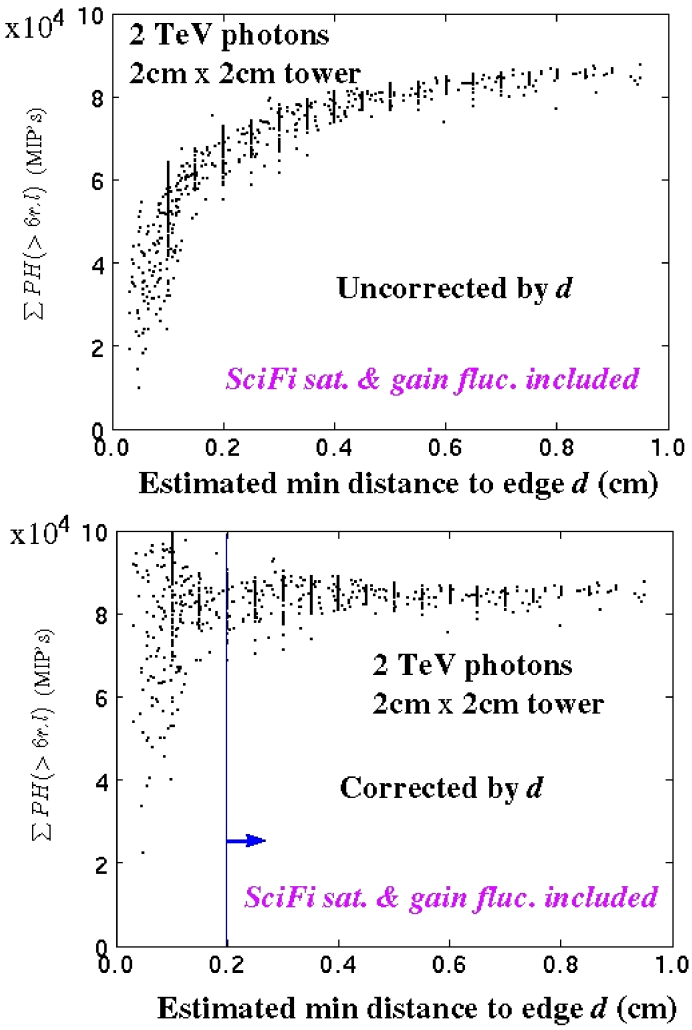

Figure 4.1: Example of the shower leakage function for 2 TeV γ-rays for the 20 mm$\times$20 mm calorimeter. The upper plot shows the number of shower particles after 6 X_0 as a function of distance of the incident position from the nearest edge. The lower plot shows the same data after correction by the leakage function. The blue arrow shows the fiducial area where the incident shower positions are 2 mm or more from the nearest edge.

then a 30% energy resolution is expected for 6 TeV neutrons. The detection efficiency after applying the cuts discussed above is about 4%.

Position determination

The simulated position resolution of the SciFi layers for detector 1 is shown in figure 4.3. The incident shower position is estimated from the fiber with the peak signal and the adjacent 2 fibers weighted by their ADC counts. The resolution is better than 0.2 mm over the energy range of 100 GeV to 7 TeV though it worsens at higher energy due to saturation. The position resolution of the silicon layers of detector 2 was also simulated and it is 15 μm for 1 TeV γ-rays. The effect of saturation is almost negligible at this energy.

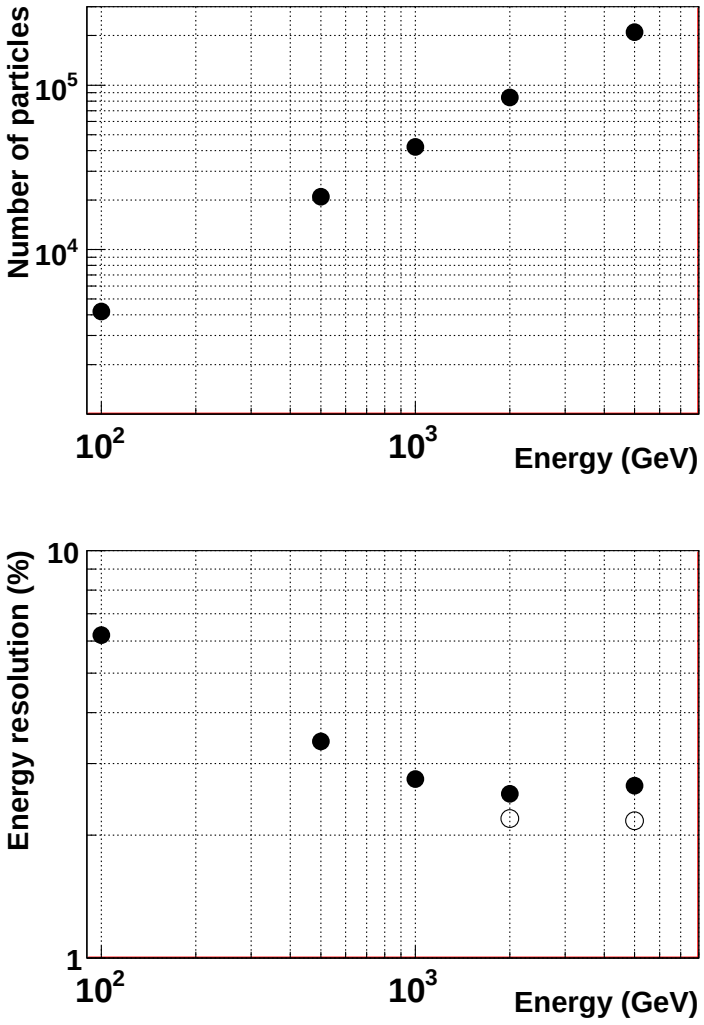

Figure 4.2: The linearity and resolution in the γ-ray energy determination. The upper plot shows number of shower particles after $6\,X_0$ and after the shower leakage correction. The lower plot shows energy resolution up to 7 TeV. Here the open circles are the data before and the filled circles after the saturation effect of the SciFi has been taken into account.

Detector geometry and acceptance

The LHCf detectors are installed between two beam pipes embedded in the TAN absorbers ± 140 m from the IP. At this location, the inner beam separation dipole has swept away all the charged secondary particles so that only neutral particles such as γ-rays from π^0 decays, neutrons or neutral kaons reach the detector. In the case of 7 + 7 TeV collisions, their flux is mostly concentrated within a few cm around the center of the neutral particle flux arriving from the IP, which is the direction of the proton beam at collision projected to the detector plane.

Figure 4.4 shows the geometrical acceptances for single γ-ray events. Here the acceptance is drawn as a function of the distance between the center of the neutral particle flux and the impact point of a particle on LHCf. Without beam crossing angle, detector 1 will locate the center of

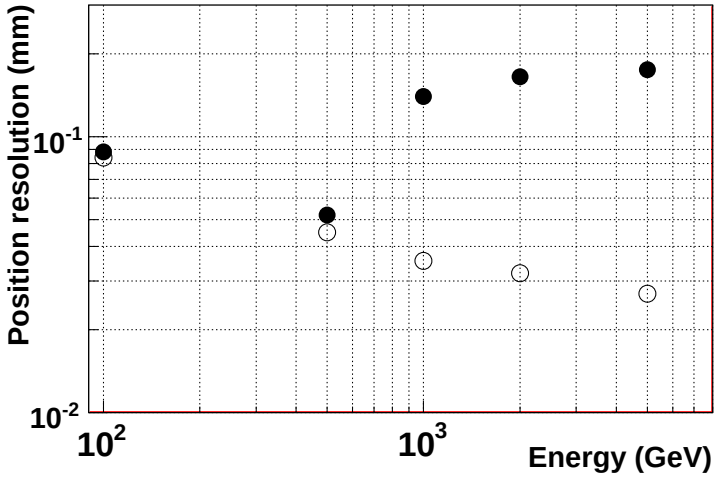

Figure 4.3: Position resolution of SciFi up to 7 TeV. The effect of saturation of the SciFi is taken into account in the filled circles but not in the open circles.

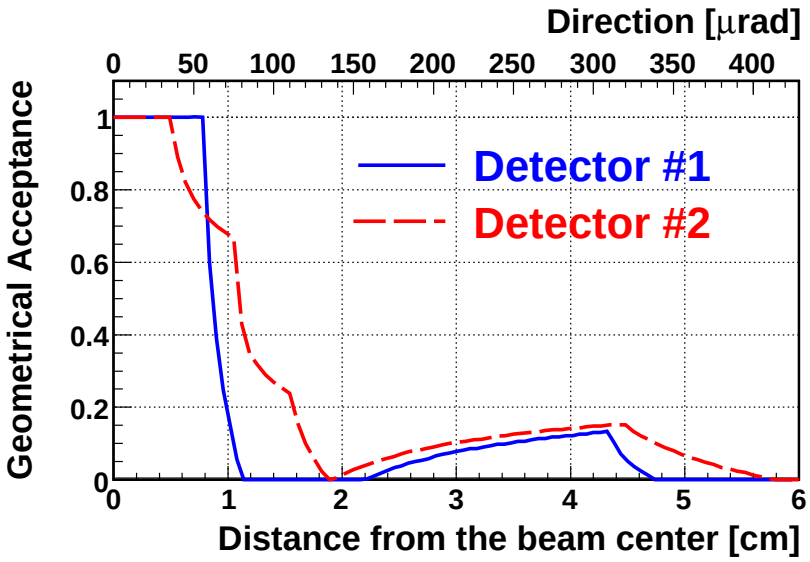

Figure 4.4: Geometrical acceptance of detector 1 (solid blue) and detector 2 (dotted red) for single γ-ray events as function of the distance from the beam axis.

20 mm×20 mm calorimeter at the center of beam-pipe where center of the flux of neutral particles exists. In this case, about half of the 40 mm×40 mm calorimeter will be cut off by the beam-pipe aperture of ±43.8 mm at the D1 magnet location. With a beam crossing angle of 140 μrad, the center of neutral particle flux moves downward by 2 cm. In this case the center of 20 mm×20 mm calorimeter will be adjusted downward by 2 cm and the P_T region covered by the detector will be enhanced.

Figure 4.5 shows the E_γ-$P_{T\gamma}$ correlation plot of photons for 7 + 7 TeV proton collisions. The curve shows the P_T acceptance of detector 1 defined by the vertical aperture of the beam pipe in the D1 magnet. The upper and the lower curves correspond to the beam crossing angles of 140 μrad

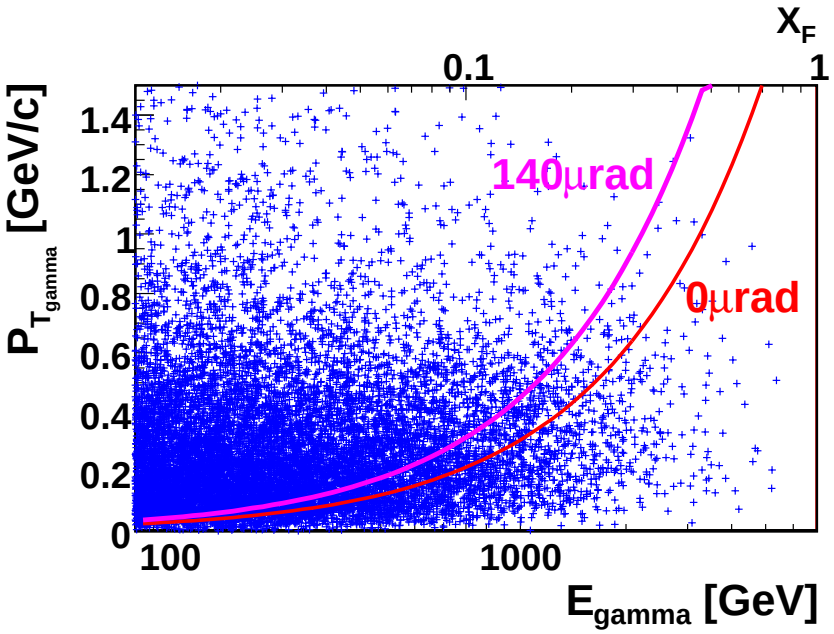

Figure 4.5: The E_γ-$P_{T\gamma}$ correlation plot. High energy photons with small P_{T_γ} can be recorded by the LHCf shower counter. The curves show geometrical cuts for our shower calorimeter arising from the configuration of the beam pipe and magnets. The upper curve (magenta) and the lower curve (red) correspond to beam crossing angles of 140 μrad. and 0 μrad, respectively.

and 0 μrad,respectively. The photons that fall in the area under the curves will be detected by LHCf. From these curves it can be seen that almost all γ-rays with energies higher than 2 TeV can be detected by LHCf.

π^0 reconstruction

The π^0 mass can be reconstructed in the invariant mass distribution of two γ-rays, one each hitting the two tower calorimeters of detector 1 or detector 2. The expected mass resolution is about 5% after taking into account 5% energy resolution and 0.2 mm position resolution.

The π^0 mass peak can be used for the absolute calibration of the energy scale. It also helps for rejection of beam-gas interactions by giving a constraint for location of the neutral pion production vertex. The acceptance of detector 1 and detector 2 for π^0 detection are shown in figure 4.6 for 1, 2 and 5 TeV. In these estimations, the crossing angle is zero and the small calorimeters are located on the horizontal midplane as shown in figure 1.4. The lower horizontal axis gives the distance between the impact point defined by extrapolation of the π^0 trajectory at production to the detector and the center of the neutral particle flux from the IP. The top horizontal axis expresses this distance as the π^0 production angle.

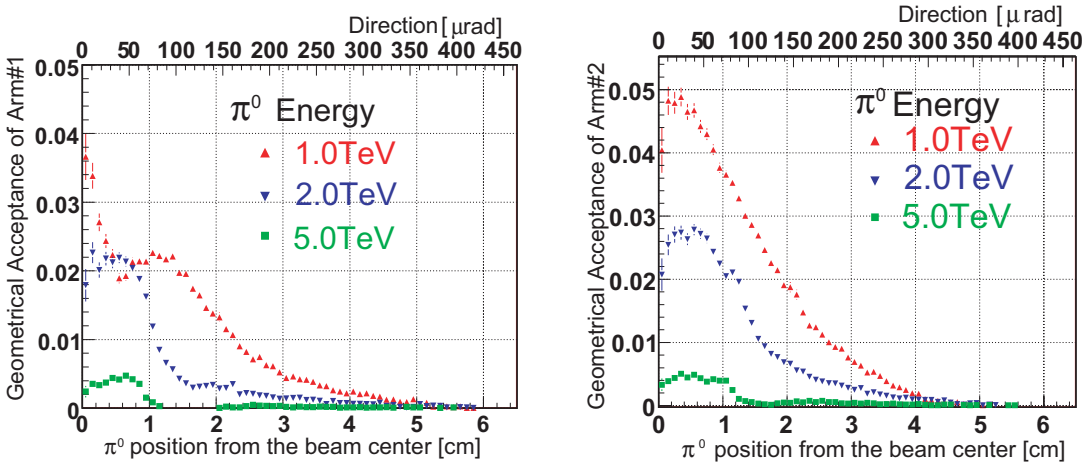

Figure 4.6: Geometrical acceptance for π^0's. Left and right plots show the acceptances for detector 1 and detector 2, respectively. Acceptances for three different π^0 energies are plotted as functions of the distance between the center of the neutral particle flux and the impact point defined by extrapolating the π^0 trajectory at production to the plane of the detector.

4.2 Results of SPS beam tests

The assembly of the detectors was finished in April 2007 and their performance was tested at the CERN SPS North Area H4 beamline from 24 August to 11 September 2007. Both detectors were exposed to electron, hadron and muon beams. Electron beams with energies of 50, 100, 150, 180 and 200 GeV, hadron beams with energies of 150 and 350 GeV and a muon beam with an energy of 150 GeV were used.

The beam test setup is illustrated in figure 4.7. One of the detectors was placed on a movable table in the beam area. Data from the calorimeters and position sensors was recorded when triggered by scintillators placed in front of the detector. At the same time, data from an external silicon strip detector (ADAMO) [22] installed between the detector and the trigger scintillators were also recorded. These data are used to precisely determine the incident position of the beam particle for comparison with the internal position sensitive layers.

In this article we briefly report preliminary results for detector 1 from the SPS2007 beam test. A detailed report on the analysis as well as results for detector 2 is in preparation.

4.2.1 Results for the calorimeters

In the beam test, the PMTs were operated at several different gains. Low gain is a default mode, in which PMTs were operated with a gain of 1 000. With this gain, the dynamic range of the calorimeters is optimized to cover 100 GeV to 7 TeV electromagnetic showers. Some higher gain modes ranging from 3 000 to 10 000 are optimized for measurements below 1 TeV with improved resolution and possibly overcoming unexpected noise in the DAQ electronics. For the muon runs, which are only available in the SPS test beam, the PMTs were operated at the highest gain of about

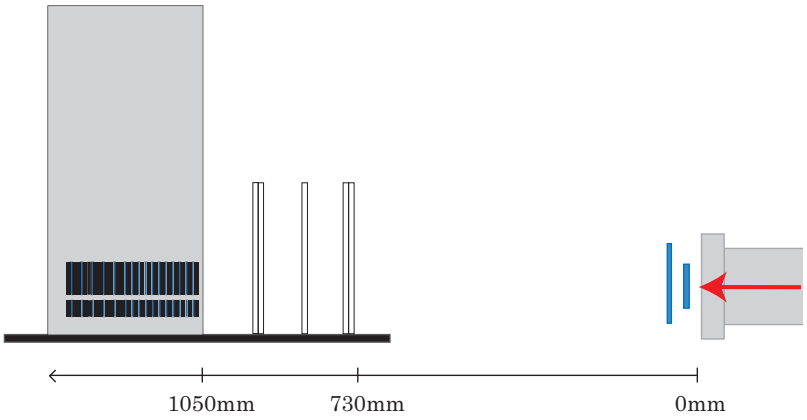

Figure 4.7: Setup of the SPS experiment. Beam enters from right along the red arrow. Two plastic scintillators indicated by blue rectangles were used to trigger beam particles. Five open rectangles show the silicon tracker, ADAMO, placed in front of the LHCf detector that is drawn as a big grey rectangle. The two black-blue structures shown in the detector are the calorimeters. The detector and ADAMO were placed on a movable stage.

10^5 to measure a single MIP. The relative gains of the different modes were measured during the pre-assembly calibration for each PMT as described in section 2.2.

The position of the shower axis was determined by the SciFi layers by finding the peak of the lateral shower shape. Gain calibration was carried out for all of the scintillating fibers in each SciFi layer. Position resolution was checked with ADAMO. The measured shower axis was used to correct for the position dependence of light yield from plastic scintillators and the shower leakage effect by referring to the previously measured non-uniformity maps and shower leakage studies.

The gain calibration of each plastic scintillator layer was carried out by using the electromagnetic showers produced by electron beams. Figure 4.8 shows an ADC distribution at the 4th layer for a 100 GeV/c electron beam. The energy that is expected from MC simulations of the shower particles is also shown. By comparing the two distributions a conversion factor from ADC to energy deposited by shower particles is determined for each layer. Conversion factors for different beam energies were obtained and are compared with each other in figure 4.10. We found these factors are consistent at the 2% level for 50 - 200 GeV electrons. To check consistency with the energy deposited by a single MIP, the muon data was analyzed as shown in figure 4.9. In this comparison, the relative PMT gain difference for the different HV settings for the electron and the muon runs was taken into account. The pedestal fluctuations of 8 AD counts (rms) due to electrical noise was also taken into account in the MC calculations. We can observe good agreement between the two distributions.

Summing up the signal in all the layers except the first, the energy resolution is defined as root-mean-square of the distribution. Here showers for which the incident particle position is reconstructed to lie $>$2 mm from the nearest edge of the calorimeter are used. The energy resolutions obtained in the beam test and in MC simulation are plotted in figure 4.11 for high gain and low gain operation. Resolution was worst for 50 GeV with low gain (450V HV) due to the electrical noise level during the SPS beam test. The electrical noise was negligible for the high gain mode

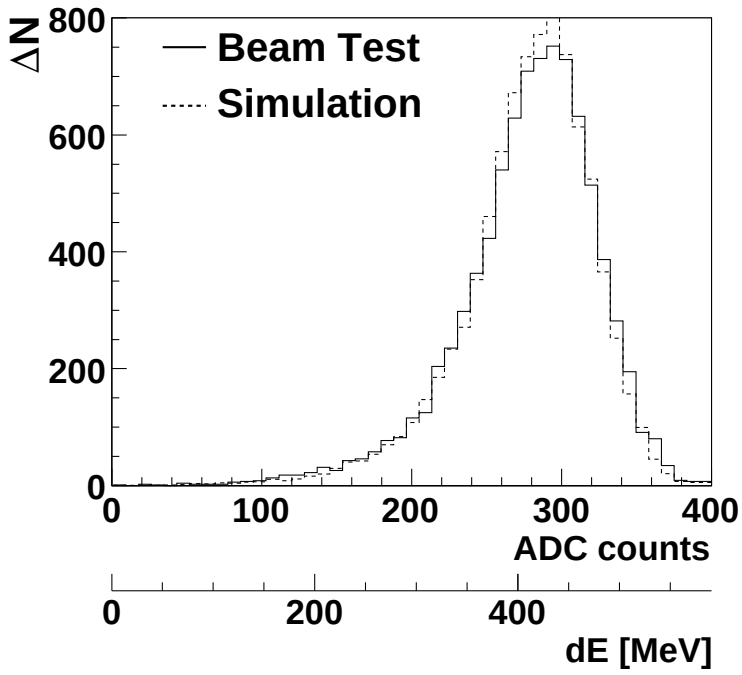

Figure 4.8: The ADC distribution at the 4th scintillation layer for 100 GeV electron showers (solid). The distribution of deposited energy expected from MC calculations (dashed) is also shown.

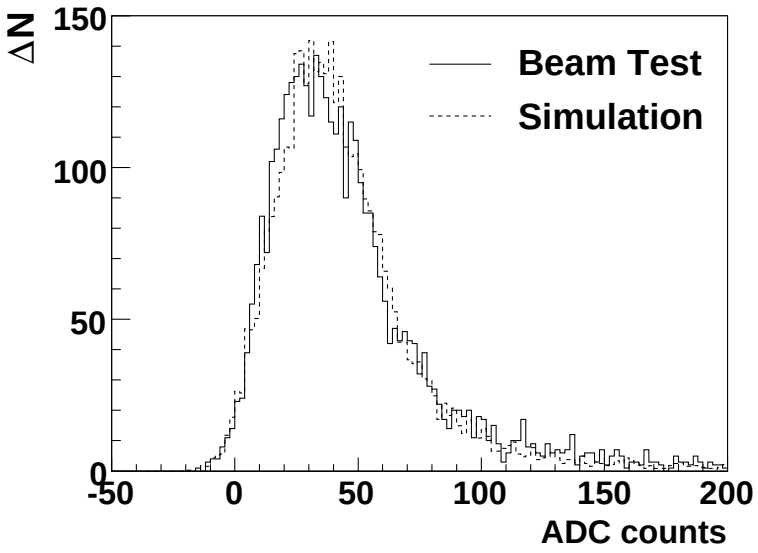

Figure 4.9: The ADC distribution at the 4-th scintillation layer for 150 GeV muon tracks (solid). The energy distribution expected from MC calculations (dashed) is also shown.

(600V HV). In any case, we have obtained excellent agreement between the data and the MC simulations showing the energy resolution is satisfactory for the experiment.

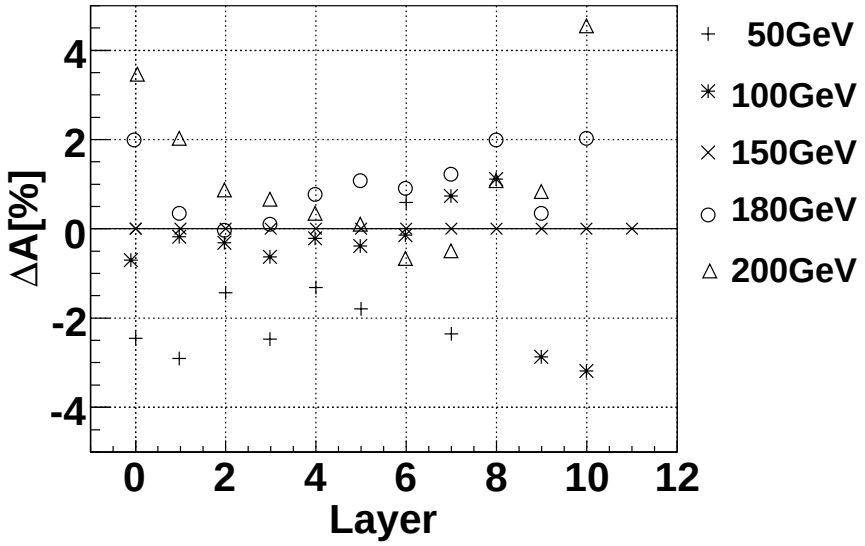

Figure 4.10: Comparison of gain conversion factors obtained from electron showers of different energy. Here the relative differences from the 150 GeV beam are shown for each layer.

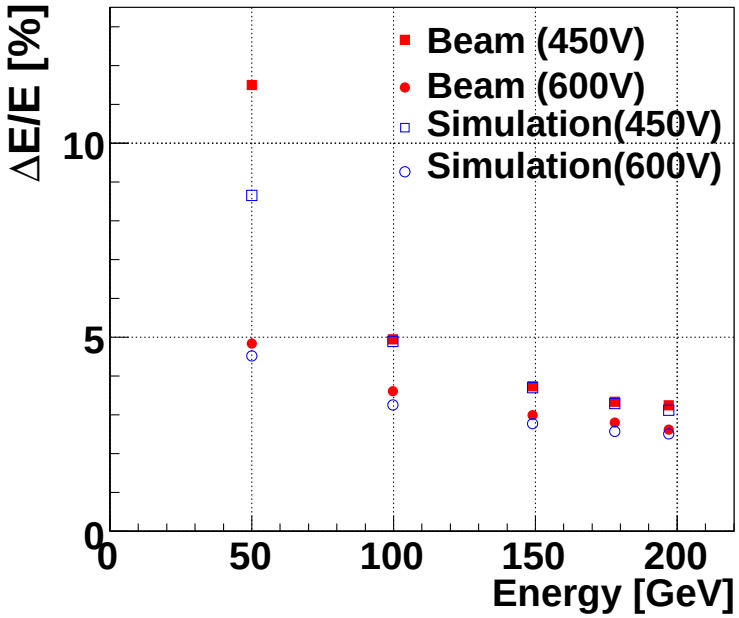

Figure 4.11: Energy resolution for electrons with two different bias HV values are given. The results of MC simulation are also plotted with blue circles.

4.2.2 Position resolution of the SciFi

The position resolution of the SciFi hodoscope used in detector 1 has been studied by using the lateral spread of electron showers at $6\,X_0$ inside the calorimeter. The position of each SciFi is calibrated beforehand by detecting a muon track which is also detected by ADAMO placed in front of the detector [22]. The center of the shower is determined from the peak signal and the signals in

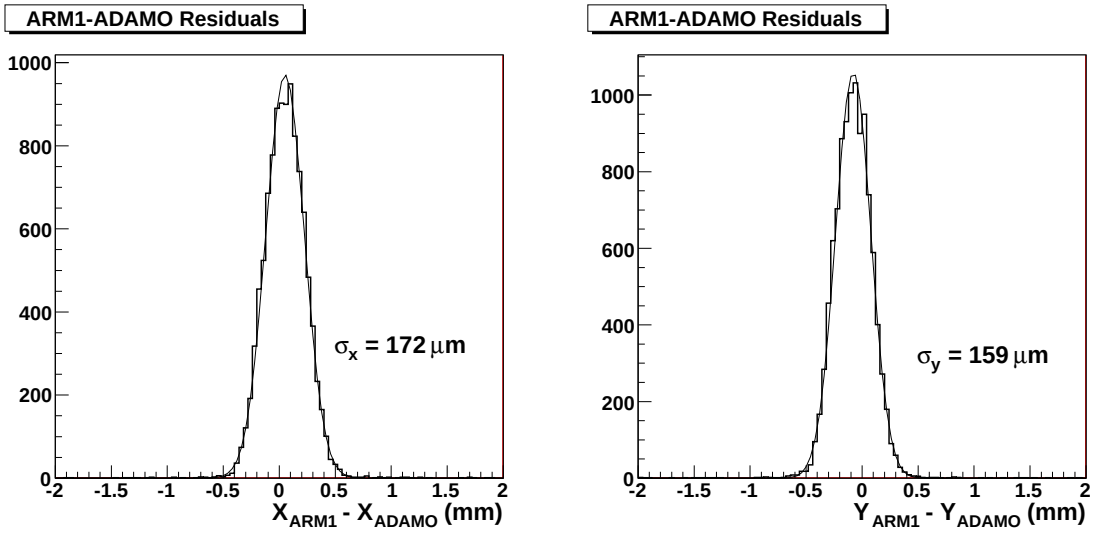

Figure 4.12: Position resolution of the SciFi in detector 1. Distributions of the difference between the shower center and incident particle position determined by SciFi and ADAMO, respectively, are plotted. The results for X and Y directions are shown in the left and right plots, respectively.

the two adjacent fibers weighted by their AD counts. The center determined by the SciFi hodoscope is compared with the incident particle position estimated by ADAMO. The distributions of the differences between these measurements in the X and Y directions are presented in figure 4.12 for 200 GeV electrons observed by the 20 mm×20 mm tower. The electron beams were uniformly scanned over the surface of the calorimeter, and the events >2 mm from the nearest edge were selected for this analysis. The distributions can be fit by Gaussian distributions with a standard deviation of σ_x=170 μm and σ_y=160 μm. The same analysis has been carried out for electron beams of 50, 100, 150 and 180 GeV. The resolution becomes slightly better with increasing energy from 200 μm to 170 μm in the X direction and from 210 μm to 160 μm in the Y direction. The analysis for the 40 mm×40 mm tower was done at an electron beam energy of 100 GeV, and the resolution obtained was 170 μm in the X direction and 230 μm in the Y direction. The results are very close to the 0.2 mm desired position resolution for energy above 100 GeV. Mis-alignment information between the LHCf detector and ADAMO has not yet been taken into account, hence an improvement in resolution is expected.

4.2.3 Position resolution of the silicon tracker

The silicon based tracker of detector 2 allows for a very good reconstruction of the γ-ray impact point on the calorimeter, that improves with increasing the γ-ray energy. From a MC simulation of the system, we calculated an expected impact point reconstruction resolution better than 100 μm for photon energy greater than 100 GeV.

A very preliminary data analysis has been done to give an estimate of the spatial resolution for the silicon based system of detector 2. This analysis was done using ADAMO for the reconstruction of the trajectory of each particle hitting the calorimeter. ADAMO was designed measuring the trajectories of single minimum ionizing particles.

2008 JINST 3 S08006

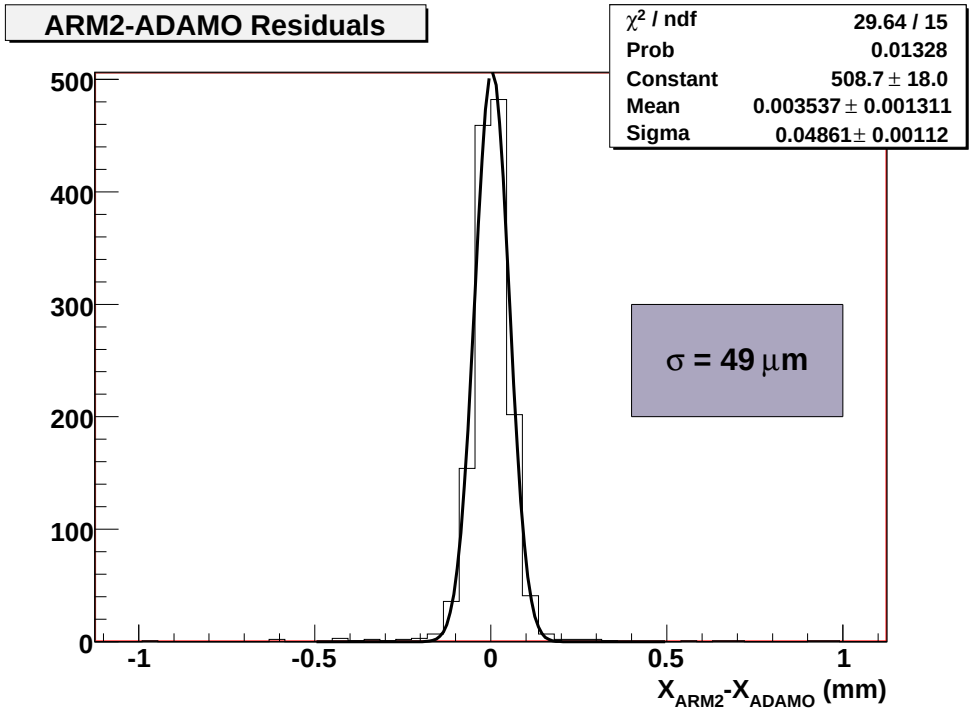

Figure 4.13: Position resolution of the silicon strip sensor in detector 2. Distribution of the differences between the measured positions of the shower centers of 200 GeV electrons at 6 X_0 inside the calorimeter and the impact points extrapolated at the same depth by using the ADAMO tracker.

Figure 4.13 shows the distribution of the differences between the measured positions of the shower centers on the LHCf silicon layer located at 6 X_0 inside the calorimeter and the impact points extrapolated at the same depth by using the ADAMO tracker. A data set of 200 GeV electrons events has been used for this analysis. Because the ADAMO system has an intrinsic spatial resolution of a few μm for minimum ionizing particles, the width of this distribution is dominated in good approximation by the LHCf silicon spatial resolution. These first results show therefore that the center of a 200 GeV e.m. shower can be reconstructed on the silicon layer located at 6 X_0 inside the calorimeter with a spatial resolution of about 50 μm.

4.2.4 Demonstration of π^0 mass reconstruction capability

To demonstrate the capability of the LHCf detectors for π^0 mass reconstruction, an experiment was performed at the SPS H4 test beam with detector 1. To produce π^0's, a carbon target of 60 mm thickness was placed 10 m in front of the detector and the target was exposed to a 350 GeV proton beam. With this geometry and energy, we can expect typically 20 GeV γ-ray pairs entering in the calorimeters. The PMTs were operated at 800 V. With this voltage the gain is 40 times higher than the gain at the nominal voltage of 450 V. To trigger on gamma-ray pairs, the trigger logic was set so that both calorimeters were required to have signals corresponding to more than 40–80 MIPS in

2008 JINST 3 S08006

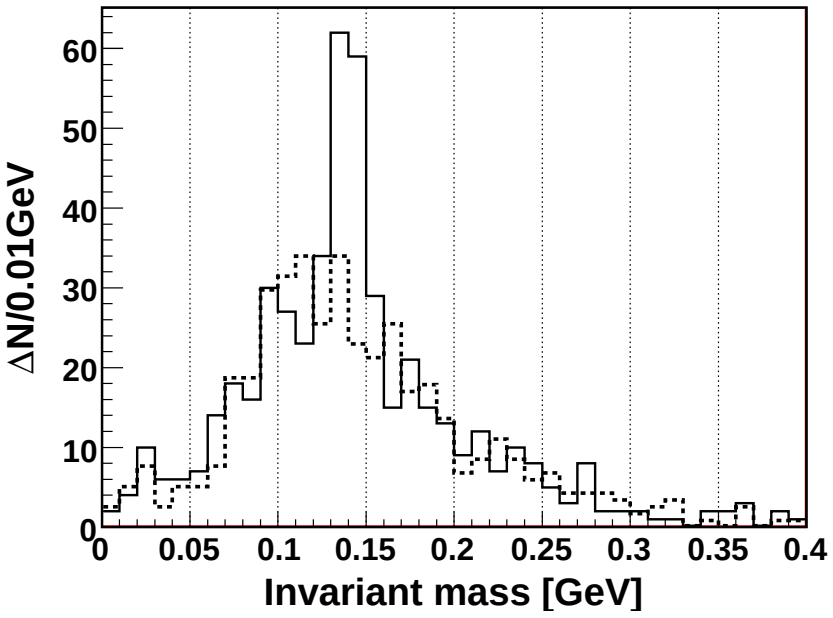

Figure 4.14: Invariant mass distribution calculated from the γ-ray pairs observed in the SPS test beam. A clear peak at the mass of π^0 (135 MeV) implies the calibration and analysis procedure were working correctly. The background shown in the dashed histogram was calculated by using uncorrelated γ-ray pairs.

any of the layers from 2 to 5. At the same time, to reduce the large proton background, we required that none of the last two scintillation layers in both calorimeters have a signal exceeding 20 MIPs.

After 6×10^7 protons entered the carbon target, 300 000 events generated the trigger and were recorded. Data reduction was carried out based on the processes described in the previous sections, i.e., position determination based on the SciFi data, 2 mm edge cut, correction for non-uniform light collection, leakage correction, and conversion from measured signals to energy deposited. The difference between the PMT gain in the nominal beam tests and in this special run was also accounted for based on the laser calibration data. Clear γ-ray pairs, each having energy more than 20 GeV, are identified in 0.6% of these recorded events. From the energies and the transverse positions of the pair, the invariant mass was calculated. The invariant mass distribution is shown in figure 4.14. A clear peak at the mass of the π^0 (135 MeV) implies the calibration and analysis procedure are working correctly. The background is caused by uncorrelated pairs those accidentally hit the two calorimeters simultaneously. The background distribution was evaluated by shifting the events in the two calorimeters so that any correlated pairs disappear. The result is also shown in figure 4.14 by dashed line and confirms the peak is really produced by π^0's. Here we note that the energy range of γ-rays in this test (20–50 GeV) was below the range that will be investigated in LHCf ($>$100 GeV).

4.3 Results of radiation damage tests

The LHCf detectors will be exposed to a considerable amount of ionizing radiation. Mokhov et al. (2003) calculated the absorbed dose distribution around the TAN [23]. Their result showed that the LHCf detector would receive a maximum radiation dose of 10 Gy/day at a nominal luminosity of $10^{29}\,\mathrm{cm}^{-2}\mathrm{s}^{-1}$. We have tested the tolerances of our plastic scintillators and clear-fiber light-guides to ionizing radiation. The test experiments were carried out with a heavy ion beam from a synchrotron at HIMAC of NIRS (National Institute of Radiological Science, Japan) and with γ-rays at the ^{60}Co Radiation Facility of Nagoya University. Effects of irradiation such as a change in the light output from the plastic scintillators and change in transparency of the light guides for the scintillation photons and also the recovery from radiation damage with time were measured.

For the heavy ion test, two kinds of plastic scintillator (EJ-260 and BC-404) and a clear-fiber light-guide (CLEARPSM, Kuraray) were irradiated with 290 MeV/n ^{12}C ion beams. Absorbed radiation dose was measured by an air ionization chamber coupled with measurements by plastic scintillators. The final integrated dose was 30 kGy with a beam intensity of 10^8 particles $\mathrm{s}^{-1}\mathrm{cm}^{-2}$. The degradation of scintillator light outputs were evaluated by measuring the signal for the weak ^{12}C beam itself and for UV light (350 nm) from a filtered Xe flash lamp (Hamamatsu L4633-01). Different irradiation rates (3×10^4 Gy/h, 8×10^4 Gy/h and increasing rate from 2×10^0 to 8×10^4 Gy/h) were compared. For γ-ray tests, similar materials were irradiated by a 100 TBq ^{60}Co source. The absorbed dose was calculated from the geometry of the source and target materials. Two dose rates (22 Gy/h and 250 Gy/h) were used by changing the distance between the source and the irradiated materials. The evaluation of the light output was done by using UV light from the Xe flash lamp. The short-term recovery of damage was also measured just after irradiation by both heavy ions and γ-rays. The long-term recovery was measured by using a radioactive beta-ray source (^{90}Sr) for several days or more. Figure 4.15 shows the variation of the scintillator and light guide light outputs for irradiation by heavy ions and γ-rays. The scintillator light outputs are almost constant up to ten Gy of absorbed dose and then decrease to 90% of the pre-irradiation value at 100 Gy or more. Most samples show a decrease of light output to 40% of the pre-irradiation value at the maximum absorbed dose of 30 kGy. There was no significant difference in the effects of irradiation measured by UV light or by the ^{12}C beam. Irradiation of the fiber light-guide showed a small decrease of light transmission for the wavelength of 490 nm because of the decrease in transparency due to irradiation. The measurement for irradiation by γ-rays showed a decrease of light output similar to that for heavy ions. The light output decreases to 90% of the initial value around 100 Gy and to 80% at 500 Gy. The damaged scintillators showed a tendency to recover within a few hours after finishing the irradiation, but the extent of recovery was very small. After one day or more, a clear recovery was observed and the light output increased from $\sim$40% to $\sim$60% of the initial light output before irradiation.

In conclusion, the plastic scintillators can be damaged by irradiation with heavy ions and γ-rays but the decrease of the light output is not large for doses of interest for LHCf. No significant dependence of radiation damage on the type of scintillator, the type of radiation, the irradiation rate, and so on were observed. Partial recovery of decreased light output is observed over several days after irradiation. Normally, the LHCf detectors will receive a dose of several tens of Gy during one week oepration. This is enough to complete the measurements unless background event rates

2008 JINST 3 S08006

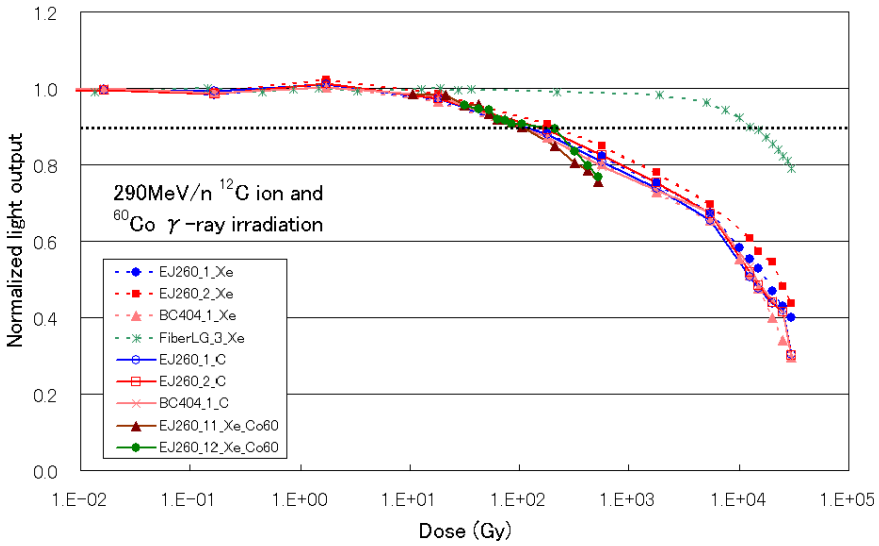

Figure 4.15: The variation of the scintillator light outputs (EJ260 and BC404) and light guide transmission for irradiation by heavy ions and γ-rays.

are very high and the run must be extended. A small decrease of light output can be corrected for by the laser calibration system and the accuracy of energy measurement will not be affected.